Tight-binding theory of interchain coupling in doped polyacetylene

H. A. Mizes and E. M. Conwell
Xerox Webster Research Center, Webster, New York 14580
(Received 10 October 1990)

Although many properties of polyacetylene, $(CH)_x$, can be qualitatively understood with a one-dimensional model, a three-dimensional model is necessary for understanding others, and for a quantitative description in any case. We formulate here a tight-binding model of three-dimensional interactions in undoped and alkali-metal-doped polyacetylene using the structures determined by x-ray diffraction. In the calculation of interchain coupling, all π orbitals on the chains are included, not just those directly opposite each other and their nearest neighbors. The coupling strength for each pair is calculated from a semiempirical relation due to Harrison, and extrapolated, again semiempirically, beyond typical interatomic spacings. It is found that the interchain coupling is energy dependent, being much stronger at the valence-band minimum than at higher energies. The calculations show that, if the Coulomb potential of the ions were absent, the potassium-doping levels required to give rise to metallic $(CH)_x$ would be greater than 15%, thus much greater than the experimental value. Dispersion relations perpendicular to the chain are derived for undoped, sodium-doped, and potassium-doped $(CH)_x$ in the "metallic" regime by means of an approximate treatment of interchain coupling. Corrections are calculated to the density of states versus energy for chain-chain coupling and doping ion-chain coupling. The ion-chain coupling is found to be of the same order of magnitude as chain-chain coupling because the larger orbital overlap between carbon atoms and doping ions than between interchain carbons is balanced out by the energy difference between these orbitals.

I. INTRODUCTION

The electronic structure of polyacetylene, $(CH)_x$, is well approximated for many purposes without including the interactions between neighboring chains. This is justified by the large material anisotropy. The average spacing between two carbon atoms in the same chain is 1.4 Å, while the spacing between the closest carbon atoms on adjacent chains is 3–4 Å, leading to an electronic coupling that is at least a factor of 10 less in the direction perpendicular to the chains than in the chain direction. The Peierls transition and the energetics and mobility of solitons and polarons arise in a one-dimensional model.[1]

However, there are many other important properties of polyacetylene whose understanding requires a three-dimensional model of the material. X-ray scattering measurements show that there is a variety of three-dimensional ordered structures for various dopant concentrations and species. Although the existence of solitons and polarons is predicted by a one-dimensional model, it has been found that the presence of solitons on a neighboring chain may hinder soliton motion.[2–4] Also, the polaron is found to be unstable when interchain coupling becomes larger than some critical value.[2,5] For doped materials, three-dimensional effects are expected to be even more important.[6] Transport of electrons in this material depends on interchain effects as well as on intrachain effects.

In this article we use tight-binding theory to estimate the strength of interchain effects in undoped, sodium-doped, and potassium-doped $(CH)_x$. The calculations are performed for a variety of dopant concentrations. We include calculations for undoped $(CH)_x$ in order to compare our results to those in the literature. We begin with a discussion of our model for estimating interchain coupling. The model gives numbers for all the geometries we consider and allows one to assign numbers to other parametric models. We go on to emphasize three different outcomes of our calculations. First, we discuss the energy dependence of the interchain coupling, and specifically, why the coupling between valence-band (VB) states is larger than that between conduction-band states. Second, we discuss how interchain coupling can give rise to a mechanism for the metal-insulator transition, finding that it is feasible only at the highest dopant concentrations. Lastly, we give a prescription for calculating the effects of chain-chain and dopant-chain interactions on the density of states for a crystal of finite chains, and present the density of states for Na-doped and K-doped $(CH)_x$.

II. MODEL OF THREE-DIMENSIONAL INTERACTIONS

Three-dimensional interactions in undoped $(CH)_x$ have been considered by a number of researchers.[2–5,7–15] The three-dimensional band structure was calculated using a self-consistent pseudopotential by Grant and Batra,[7] using a linear-muffin-tin-orbital (LMTO) potential by Ashkenazi *et al.*,[8] and using a first-principles local-density-functional pseudopotential by Vogl and Campbell.[5] The

 ©1991 The American Physical Society

total energy of the three-dimensional crystal has also been considered by Vogl and Campbell, as well as by Baughman *et al.*,[9] who used pair potentials to minimize the lattice energy, and by Stafström, who used the modified neglect of differential orbitals (MNDO) to minimize the total energy.[10]

Kertesz has considered the electronic structure of potassium- and iodine-doped $(CH)_x$ using the extended Hückel model.[15] His calculations show there is almost a complete transfer of charge from the dopant to the chain, in agreement with earlier single-chain calculations by Brédas.[16] He goes on to calculate the perpendicular bandwidths for doped materials. His calculations do not, however, include the Peierls dimerization. In addition, a Gaussian smoothing procedure smears the density-of-states calculation by 0.5 eV, which makes studying phenomena that occur on a smaller energy scale impossible.

The stability and confinement of polyacetylene's elementary excitations (solitons, polarons, and bipolarons) due to three-dimensional interactions have been studied by extending the Su-Schrieffer-Heeger[1] (SSH) and Takayama–Lin-Liu–Maki[17] (TLM) models of $(CH)_x$ to allow for interchain coupling. Baeriswyl and Maki have studied interchain effects by introducing a term in a two-chain Hamiltonian that couples atoms directly opposite each other.[3] They have allowed this term to alternate in magnitude to allow for the zigzagging of the chain.[2,4] A similar approach to studying the three-dimensional nature has also been used by other groups.[2–4,11–14]

Our model is similar to these latter models in that we extend the SSH formalism to allow hopping of the electron between chains. However, we include a number of additional features that enable us to do more accurate calculations and, further, to describe doped crystals. In the SSH-based models, the perpendicular coupling is described by a single parameter $t_\perp$, or at most a few parameters.[12] Our model uses the observed crystalline structures of the undoped and doped material to calculate an effective $t_\perp$ that depends on energy as well as on the orientation of the two chains being coupled. In some of our calculations we also include coupling between the dopant s orbitals and the carbon p_z orbitals, and the Coulomb potential that the carbon atoms feel due to the charged ions.

To be more explicit, the Hamiltonian we use is

$$H = H_{\rm SSH} + H_{\rm Coul} + H_{c\text{-}c} + H_{c\text{-}d} + H_d \ . \tag{1}$$

In Eq. (1), $H_{\rm SSH}$ denotes the electronic terms of the SSH Hamiltonian,[1] $H_{\rm Coul}$ is the Coulomb potential acting on a chain due to the doping ions and charged solitons on other chains, $H_{c\text{-}c}$ are the terms that couple the polyacetylene chains, $H_{c\text{-}d}$ are the terms that couple the chains to the dopants, and H_d are the orbital energies of the dopants. We consider each of the terms of H in turn. We take $H_{\rm SSH}$ to be[1]

$$H_{\rm SSH} = \sum_{m=1}^{M_c} \sum_{n=1}^{N_c} \{ \varepsilon_n c_{nm}^\dagger c_{nm} - [t_0 + \alpha(u_n - u_{n+1})] \times (c_{n+1,m}^\dagger c_{nm} + \text{H.c.}) \} \ . \tag{2}$$

Here u_n is the displacement of the nth lattice site from its location in the uniform chain; t_0 is the transfer integral when $u_n = 0$ for all n; α is the rate of change of the transfer integral with distance between nearest neighbors; and $c_{nm}^\dagger$ and c_{nm} are the creation and annihilation operators, respectively, for a π electron on the nth site of the mth chain. N_c is the number of sites on the chain and M_c the number of chains in the crystal. We include an additional term $\varepsilon_\pi c_{nm}^\dagger c_{nm}$, which is the energy of an electron in the π orbital. This term is neglected in the SSH Hamiltonian because that Hamiltonian was designed to study only energy shifts due to intrachain coupling. However, in doped crystals, the energy levels depend on the energy difference between the carbon atom π orbital and the dopant orbital, so we require this term.

When $(CH)_x$ is doped, the low value of Pauli susceptibility χ_P for dopant concentration y up to ~ 4–6% indicates that the extra electrons or holes go into soliton states.[18] The regular spacing of the doping ions[19–21] means that the solitons are arranged in a lattice. Doping beyond 4–6% causes χ_P to increase very rapidly.[18] There has been considerable discussion as to whether, for y beyond 4–6%, the extra electrons are arranged in a soliton lattice or a polaron lattice. The principal evidence against the latter is the observation that the intensity of the three doping-induced infrared-absorption lines (IRAV) increases more or less linearly with doping in K-doped $(CH)_x$ up to $\sim 18\%$ doping.[22] It has been shown that, within the effects included in $H_{\rm SSH}$, beyond $y \sim 6\%$ the polaron lattice would be unstable.[23] Its instability is enhanced by interchain coupling[5] and by finite temperature.[24,25] It has been argued that the charge polarization associated with the polaron found in self-consistent calculations can account for the IRAV.[26] Although large effects are found for an isolated polaron, which is over 20 sites long, at 16.7% doping the polarons are only six sites long. The amplitude of the characteristic distortion decreases drastically then,[23] and the charge polarization must decrease accordingly. For these reasons and others,[27–29] we take it that in doped polyacetylene for any y above a few tenths of a percent, the charges are arranged in a soliton lattice. The presence of N_s solitons on the chain is incorporated into our calculation by taking

$$u_n = -(-1)^n u_0 \sum_{j=1}^{N_s} \tanh\left[\frac{n - jb}{l} \right] , \tag{3}$$

where u_0 is the displacement in the perfectly dimerized chain, b the spacing between soliton centers, and l the half-length of the soliton.

Although a soliton lattice was assumed for calculating the wave functions for individual chains in doped samples, we simplified the calculation of interchain interactions by assuming a uniform distribution of C-H's on the chain. This has an insignificant effect on our estimate of the strength of the interchain coupling. While changing the interatomic spacing by 0.14 Å (the length difference between single and double bonds) changes the intrachain coupling by 0.9 eV, or approximately 35%, the same displacement changes the interchain coupling by less than 1%. This is primarily due to the displacements being

perpendicular to the interchain spacing. Therefore, the interchain coupling should, to the accuracy of the present calculation, be the same for an undimerized chain, a soliton lattice, or a polaron lattice.

H_{Coul} is the Coulomb potential induced by neighboring ions and solitons and is given by

$$H_{\text{Coul}}=\sum_{m=1}^{M_c}\sum_{n=1}^{N_c} V_{nm}c_{nm}^{\dagger}c_{nm} \ , \tag{4}$$

where V_{nm} is the Coulomb potential felt by the nth atom in the mth chain. Since the location of the ions and solitons has been taken the same for each ion column and $(CH)_x$ chain, V_{nm} is independent of m. We have discussed the importance of this term in previous publications.[27–29] The strength of this interaction can be as large as 5 eV, the value found for 16.7% K-doped $(CH)_x$.[28] We have found that, because it is energetically favorable for the ions to avoid the ends of the chains, a potential well with a depth of the average V_{nm} is formed along the $(CH)_x$ chain and the presence of this well makes significant shifts in the band structure near the Fermi level. These shifts lead to a partially filled band and thus metallic behavior for heavily doped material. Although we show that interchain coupling can give rise to an insulator-metal transition, we find that this mechanism is only significant for the most heavily doped materials. We therefore find it necessary to include the Coulomb interactions to give metallic bands at doping $y \geq 6\%$.

In Fig. 1 we show the crystalline geometry we use for undoped polyacetylene,[30] Na-doped $(CH)_x$,[31] and K-doped $(CH)_x$.[20] The diffraction results show that the ions go into columns parallel to the chains, and as more ions are incorporated into the lattice, the spacing between the ions decreases. In our model crystals we take all the chains to be the same length and all the ion columns to be the same length.

$H_{c\text{-}c}$ is the term in the Hamiltonian that couples orbitals between any two chains and is given by

$$H_{c\text{-}c}=\sum_{m=1}^{M_c}\sum_{n=1}^{N_c}\sum_{m'=1}^{M_c}\sum_{n'=1}^{N_c} t_{nm,n'm'}^{c\text{-}c}(c_{nm}^{\dagger}c_{n'm'}+\text{H.c.}) \ . \tag{5}$$

Because the coupling between orbitals is exponentially dependent on the separation between them, only atoms on neighboring chains couple significantly, and we set $t_{n,m,n'm'}=0$ when m and m' are not nearest neighbors. To be more explicit, we consider coupling to only the six neighboring chains in undoped polyacetylene, the six neighboring chains in the sodium geometry, and the four neighboring chains in the potassium geometry, as indicated in Fig. 1.

Coupling to a neighboring chain atom directly opposite a particular atom ($n=n'$) is not the only significant coupling. It has been shown that non-nearest-neighbor transfer integrals between sites that are chemically bonded in transannular molecules (molecules containing two sections that are separated by few angstroms) significantly alter the excited-state spectra.[32] Interchain interactions in polyacetylene are of a similar nature. We will show that the non-nearest-neighbor couplings weaken the interchain interactions at the Fermi energy.

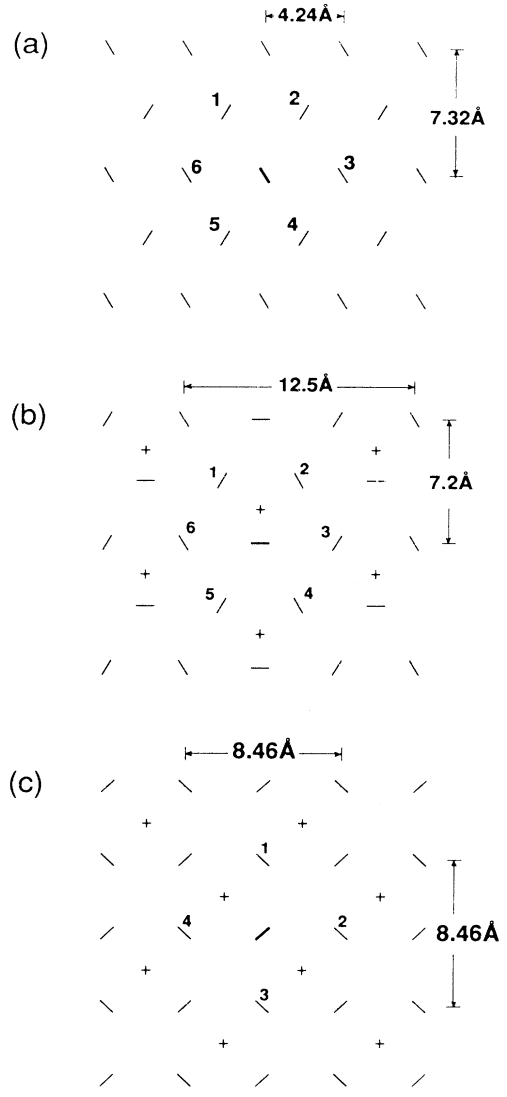

FIG. 1. Three-dimensional crystal structures of the three types of polyacetylene we consider in this paper. The lines represent the polyacetylene chains coming out of the paper, while the plus signs represent the ion columns. (a) Undoped polyacetylene, (b) sodium-doped polyacetylene, (c) potassium-doped polyacetylene. The nearest-neighbor chains to the chain indicated by the heavy line are numbered in the figure.

In Fig. 2 we show the geometry involved in calculating the coupling between the two p orbitals. The coupling depends on both the separation $\mathbf{d}$ between the orbitals and on their relative orientation. Let $\mathbf{v}_1$ and $\mathbf{v}_2$ be vectors pointing from the origin of the two orbitals in the direction of the positive lobes, and let Φ_1 and Φ_2 be the angles these vectors make with $\mathbf{d}$. If $\mathbf{v}_1$ were pointed at the origin of orbital 2, while $\mathbf{v}_2$ were perpendicular to $\mathbf{v}_1$, then the symmetry of a p orbital would give a zero coupling energy. On the other hand, the coupling energy would be

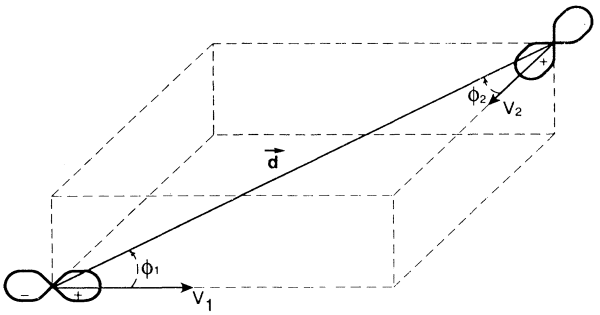

FIG. 2. Geometry for the orientational dependence of the coupling between two p orbitals.

a maximum for $\mathbf{v}_1$ and $\mathbf{v}_2$ pointed at each other. The orientation of any two polyacetylene p orbitals lies in between these two extremes for the crystal structures in Fig. 1.

To calculate the coupling between two p orbitals, it is useful to replace each one by a linear combination of two suitably chosen p orbitals. One set is chosen so that $\mathbf{v}_1$ and $\mathbf{v}_2$ are pointing at each other (σ coupling) and the other so that $\mathbf{v}_1$ and $\mathbf{v}_2$ are parallel and perpendicular to $\mathbf{d}$ (π coupling). The sum of the σ-oriented orbital and the π-oriented orbital gives the original orbital, so this description is equivalent. Harrison has proposed a semiempirical relation that gives an estimate of σ and π couplings.[33] According to this relation, the coupling strength V for either is

$$V=\eta\frac{\hbar^2}{md^2}\ , \tag{6}$$

where m is the electron mass, d is the orbital separation, and η is a parameter that is 2.22 for σ bonding and -0.63 for π bonding.[34] When we estimate the intrachain coupling with this formula, using the actual distance of 1.4 Å between intrachain carbons, we find that $V=2.4$ eV, which is close to the commonly accepted value for t_0 of 2.5 eV. We will continue to use 2.5 eV for the intrachain coupling, while using the estimates of Eq. (6) for the interchain coupling.

Harrison's formula holds only for d of the order of interatomic spacing in an isotropic solid. For larger distances the coupling is expected to fall off exponentially with d. We therefore write for large distances

$$V=Ae^{-\mu d}\ . \tag{7}$$

The inverse decay length μ can be estimated from the binding energy ε_π of a p orbital electron, which has been calculated to be -11.07 eV.[34] Using $\mu=(2m\varepsilon_\pi/\hbar^2)^{1/2}$, which is the rate at which a bound state of energy ε_π decays in vacuum, we find $\mu=1.70$ Å^{-1}. A can be found by matching Eq. (7) to Eq. (6) for $d=1.54$ Å, the nearest-neighbor spacing in diamond. When this is done separately for π and σ coupling, we find a general expression for the coupling in eV of any two p orbitals for $d>1.54$ Å, which is

$$t_{nm,n'm'}=(98.5\cos\Phi_1\cos\Phi_2 - 27.9\sin\Phi_1\sin\Phi_2\cos\theta)e^{-1.70d}\ , \tag{8}$$

where θ is the angle between the projections of $\mathbf{v}_1$ and $\mathbf{v}_2$ in a plane perpendicular to $\mathbf{d}$.

H_d and $H_{c\text{-}d}$ are the parts of the Hamiltonian that describe the dopants and their coupling to the chain and are given by

$$H_{c\text{-}d}=\sum_{m=1}^{M_c}\sum_{n=1}^{N_c}\sum_{m'=1}^{M_d}\sum_{n'=1}^{N_d} t^{c\text{-}d}_{nm,n'm'}(c^\dagger_{nm}d_{n'm'}+\text{H.c.})\ , \tag{9}$$

$$H_d=\sum_{m=1}^{M_d}\sum_{n=1}^{N_d}\varepsilon_d d^\dagger_{nm}d_{nm}\ . \tag{10}$$

N_d is the number of dopant ions in an ion column, and M_d is the number of ion columns. $d^\dagger_{nm}$ and d_{nm} are the creation and annihilation operators, respectively, for an electron on the nth ion of the mth column. Because we are considering only alkali-metal-atom doping, only the valence s orbital is included in the Hamiltonian. ε_d is the energy of this s orbital. $t^{c\text{-}d}_{nm,n'm'}$ gives the coupling of the nth orbital on the mth $(CH)_x$ chain to the nth ion in the mth column. We estimate the coupling between ions and dopants in a similar manner to that for interchain coupling. We use Eq. (6), with η chosen as the universal parameter for sp coupling (equal to 1.42)[34] and d the distance between an ion and the nearest chain atoms. The exponential form, Eq. (7), is matched to Eq. (6) for coupling to carbon orbitals further from the ion. There is a difference in ion coupling for potassium- and sodium-doped materials because of both the different geometries and ε_d's (and thus μ's) for sodium and potassium. We find again that ion coupling to carbons other than those directly opposite the ion is significant. However, we find significant coupling only to nearest-neighbor chain atoms—that is, the potassium ion is coupled only to the four neighboring chains, and the sodium ion is coupled only to the three neighboring chains.

III. ENERGY DEPENDENCE OF PERPENDICULAR COUPLING

Let us define a plane that is perpendicular to all the $(CH)_x$ chains and that contains the π orbital to which the coupling is being calculated. Equation (8) predicts that not only is the coupling between this atom and those on nearest-neighbor chains in the plane significant, but also the coupling between this atom and those on nearest-neighbor chains in planes that are parallel to the first plane. In Table I we give the coupling for undoped polyacetylene in the $P2_1/a$ structure with the dimensions of the crystal taken from Fig. 1 of Ref. 30. We tabulate the couplings between the two nonequivalent atoms, labeled a and b, in a single chain and the atoms in the six nearest-neighbor chains [see Fig. 1(a)] that are within $|n-n'|=2$ of this chain atom. The direction of the positive lobe on the p_z orbital is chosen to give the valence-band minimum at the center of the Brillouin zone, as will

TABLE I. Coupling between atom pairs on neighboring chains in undoped polyacetylene.

Chain	Atom	Coupling to opposite atom (eV)	Coupling to atom one site up (eV)	Coupling to atom two sites up (eV)
1	a	−0.0657	−0.0329	−0.0138
2	a	−0.0135	−0.0329	−0.0034
3	a	0.0101	0.0005	0.0008
4	a	−0.0135	−0.0140	−0.0034
5	a	−0.0657	−0.0140	−0.0138
6	a	0.0101	0.0296	0.0008
1	b	−0.0135	−0.0140	−0.0034
2	b	−0.0657	−0.0140	−0.0138
3	b	0.0101	0.0296	0.0008
4	b	−0.0657	−0.0329	−0.0138
5	b	−0.0135	−0.0329	−0.0034
6	b	0.0101	0.0005	0.0008

be seen. The coupling to an atom at $|n-n'|=1$ can be larger because the zigzag of the chains can cause this atom to be closer than the one directly opposite. In fact, the coupling to the atom directly opposite can account for less than 30% of the coupling between that atom and the other chain. The interchain coupling is larger between nonequivalent chains than between equivalent chains, but both couplings are of the same order of magnitude.

Baeriswyl and Maki[4] and Fesser[12] have used tight-binding theory to discuss the energetics of different crystalline arrangements of the polyacetylene lattice. In order to quantify their calculations, Baeriswyl and Maki neglected coupling between equivalent chains and introduced the interchain coupling parameters t_1 and t_2. The coupling between two chain atoms directly opposite each other was taken alternatively as t_1+t_2 and t_1-t_2. Fesser considered in addition the coupling between a chain atom and the nearest neighbors to the atom directly opposite, taking this coupling to be alternatively r_1+r_2 and r_1-r_2. The variation between couplings of adjacent pairs of atoms occurs because of the zigzag of the chain. In terms of our interchain coupling parameters, Eq. (5), t_1, t_2, r_1, and r_2 are given by

$$t_1=\tfrac{1}{2}(t^{c\text{-}c}_{n,m;n,m'}+t^{c\text{-}c}_{n+1,m;n+1,m'}) , \tag{11}$$

$$t_2=\tfrac{1}{2}(t^{c\text{-}c}_{n,m;n,m'}-t^{c\text{-}c}_{n+1,m;n+1,m'}) , \tag{12}$$

$$r_1=\tfrac{1}{2}(t^{c\text{-}c}_{n,m;n+1,m'}+t^{c\text{-}c}_{n-1,m;n,m'}) , \tag{13}$$

$$r_2=\tfrac{1}{2}(t^{c\text{-}c}_{n,m;n+1,m'}-t^{c\text{-}c}_{n-1,m;n,m'}) , \tag{14}$$

where m' and m index nearest-neighbor chains. Note that coupling strength does not alternate for atoms on equivalent chains because $t_2=0$.

We use Eq. (8) to calculate t_1, t_2, r_1, and r_2 for the six nearest-neighbor chains in undoped polyacetylene and give them in Table II. The condition $|t_2|>|t_1|$ required for Baeriswyl and Maki's calculation to lead to parallel bond ordering on inequivalent chains[4] is not satisfied. Thus their calculations lead to out-of-phase ordering, in disagreement with the experimental results.[30] Fesser's calculations lead to out-of-phase ordering of the dimerization for the equivalent chains, also in disagreement with experiment. The failure of these calculations might be a result of energy calculations not being extendable to 3D structures, where all possible perpendicular wave vectors must be considered to calculate total energy. However, a more plausible explanation, in line with the results of Vogl and Campbell,[5] is that the total energy is strongly influenced by orbitals other than the carbon p_z.

One might think that because the tight-binding model is parametric, one could increase the coupling between atoms with $n=n'$, while setting all couplings with $n\neq n'$ to zero, and obtain the same results. However, this is not the case. Because the orbitals with $n\neq n'$ significantly couple, there is an energy dependence to the effective coupling between chains. To make this quantitative, it is useful to define an effective perpendicular coupling between chains m and m',

$$t_{\perp,mm'}(E)=\sum_{n=1}^{N_c}\sum_{n'=1}^{N_c} c_n(E)c_{n'}(E)t^{c\text{-}c}_{nm,n'm'} , \tag{15}$$

where the c_n are the normalized coefficients of the atomic orbital for the eigenvalue of energy E. It was found that inclusion of nearest neighbors to the opposite atom (i.e., r_1 and r_2) accounts for over 75% of the effective perpendicular coupling between chains.

TABLE II. Interchain coupling parameters for undoped polyacetylene.

Chain	t_1 (eV)	t_2 (eV)	r_1 (eV)	r_2 (eV)
1	−0.0396	0.0281	−0.0235	0.0095
2	−0.0396	0.0281	−0.0235	0.0095
3	0.0101	0	0.0151	0.0146
4	−0.0396	0.0281	−0.0235	0.0095
5	−0.0396	0.0281	−0.0235	0.0095
6	0.0101	0	0.0151	0.0146

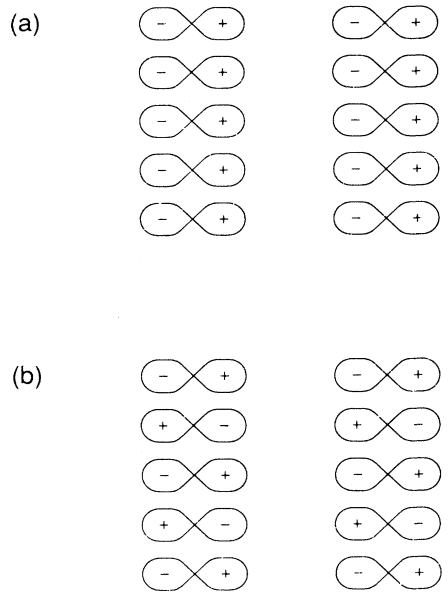

FIG. 3. Physical illustration to show why the coupling for lower-energy states is stronger than that for higher-energy states. See the text for an explanation. (a) State near the valence-band minimum; (b) state near the conduction-band maximum.

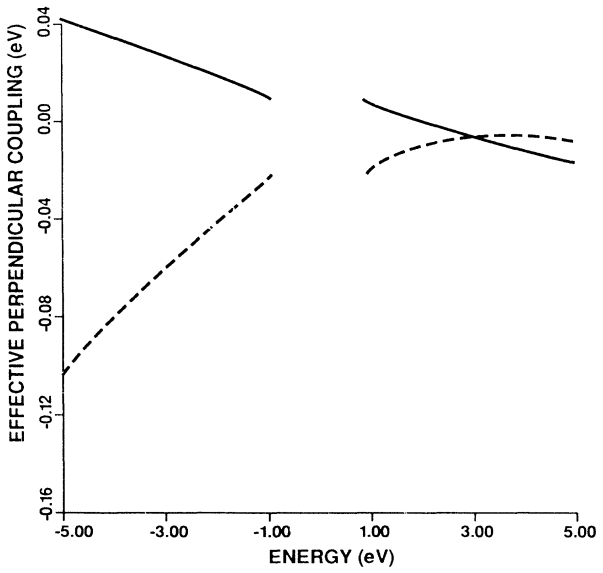

FIG. 4. Effective perpendicular coupling calculated from Eq. (15) as a function of energy for undoped polyacetylene. The solid line represents the coupling to the nonequivalent chains, while the dotted line represents that to the equivalent chains.

With regard to the energy dependence of $t_{\perp,mm'}(E)$, it is expected that valence-band states will be more strongly coupled than conduction-band states. The reason this happens is illustrated in Fig. 3. The wave function for a particular 1D eigenvalue is a linear combination of the p_z orbitals. In Fig. 3 we show (a) the signs of the tight-binding wave function for two chains with states at the bottom of the valence band, and (b) two chains with states at the top of the conduction band. The sign of the coupling for a given pair of atoms is the negative of the combined sign of the overlapping lobes. For the valence-band wave function shown, both the $n=n'$ and $n\neq n'$ couplings are positive and reinforce constructively. Therefore, the total coupling is larger than it would be if we considered just the two atoms opposite each other. For the conduction-band wave function, the couplings alternate in sign and reinforce destructively. The coupling between two conduction-band wave functions is therefore expected to be less than the coupling between two valence-band wave functions.

These expectations are borne out by quantitative calculations. In Fig. 4, $t_{\perp,mm'}(E)$ is plotted as a function of E for the two nonequivalent perpendicular couplings in undoped $(CH)_x$. The plots show the expected energy dependence, with the magnitude of the coupling being largest at the bottom of the valence band and decreasing with increasing energy. For the conduction band the coupling is generally quite small. The energy dependence shown in Fig. 4 is not an artifact of the tight-binding method, but is also seen in *ab initio* calculations. In Table III we give the perpendicular bandwidths at the bottom of the valence band and at the top of the valence band for three *ab initio* calculations obtained from the published band structures. We also include the perpendicular bandwidth from our tight-binding calculation, to be carried out in Sec. V. We see that all three of the *ab initio* calculations give a larger bandwidth at the bottom of the valence

TABLE III. Perpendicular bandwidths for different three-dimensional band-structure calculations.

Author	Type of calculation	Bandwidth at VB minimum (eV)	Bandwidth at VB maximum (eV)
Grant and Batra (Ref. 7)	Self-consistent pseudopotential	0.3	0.1
Vogl and Campbell (Ref. 5)	First-principles local-density-functional pseudopotential	0.9	0.5
Ashkenazi *et al.* (Ref. 8)	Linear-muffin-tin orbital	0.7	0.3
Mizes and Conwell	Tight-binding	0.82	0.16

band, where the couplings interfere constructively, as compared to the top of the valence band, where the constructive interference is not as strong. Our estimate of the bandwidth is comparable to that from the *ab initio* calculations.

IV. METAL-INSULATOR TRANSITION

The increase in the Pauli susceptibility observed at $\sim 4-6\%$ doping has been attributed to the sample going from semiconductor to metal. We have previously shown how the Coulomb effect of the ions may perturb the bands of a soliton lattice and give rise to a metallic density of states.[27–29] In this section, however, we wish to examine whether interchain coupling alone can give rise to this transition.

Consider the π band of an infinite chain of polyacetylene with a soliton lattice deformation in the chain. To the accuracy of the SSH or TLM Hamiltonians, the π electrons will form three distinct bands. These will consist of the valence band and the conduction band that one obtains when the chain dimerizes, plus a midgap band composed of the soliton levels. The width of this midgap band depends on the spacing between the solitons and can be calculated analytically.[35,36] However, no matter what the soliton spacing, there will always be a gap between the soliton band and the conduction and valence bands.

If we turn on the interchain coupling, however, there will be dispersion in the direction perpendicular to the bands and this will tend to close the gap. If the soliton-band maximum is close enough to the conduction-band minimum, the interchain coupling could cause the gap to go to zero, giving metallic Pauli susceptibility.

In Sec. II we described a method for estimating the strength of interchain coupling in doped polyacetylene. The Hamiltonian there describes a collection of M_c chains and M_d ion columns of length N_c and N_d, respectively. In order to obtain energy bands instead of a series of discrete eigenvalues, we modify our Hamiltonian so that it describes an infinite lattice of infinite chains. This Hamiltonian maintains the general form of Eq. (1) and associated equations, but the sum over m is not over all the chains and ion columns in the crystal, but is restricted to those in the unit cell. Coupling between the chains and ions columns in different unit cells picks up a phase factor $e^{i\mathbf{k}_\perp\cdot\mathbf{r}}$, where $\mathbf{k}_\perp$ is a perpendicular wave vector and $\mathbf{r}$ is the displacement to the next unit cell. A term including the phase factor $e^{i\mathbf{k}_\parallel\cdot\mathbf{r}}$ links the end of the chain to the beginning of the chain. In order to investigate the effect of interchain coupling alone, we remove the term H_{Coul} from the Hamiltonian. For infinite chains, this term could not give rise to a metal anyway, since a potential well would not be formed. We perform the calculations with and without the chain-dopant coupling term $H_{c\text{-}d}$.

In order to demonstrate the strength of interchain coupling required to cause the insulator-metal transition, we allow the effective coupling to vary. More explicitly, we introduce a new parameter t_{mult} that multiplies Eq. (8). We then pick a dopant density, which defines the size of our unit cell. For example, for 16.7% K-doped $(CH)_x$, the ions are spaced three sites apart. Because there are two chains per ion column, solitons on the same chain are spaced six sites apart. The solitons alternate between those that can be described schematically as having two single bonds and those with two double bonds, so the repeat distance along the chain direction is 12 sites. There are two chains and four ions per unit cell, leading to a 28×28 matrix for which the eigenvalues must be determined as functions of $k_\perp$ and $k_\parallel$. Starting with $t_{\text{mult}}=0$, we increase it until we observe the top level of the soliton band cross the bottom level of the conduction band. This t_{mult} determines the strength of the interchain coupling required to cause the transition to a metal for this particular dopant density.

In Fig. 5 we plot the phase diagram arising from the interchain coupling mechanism for the insulator-metal transition for K-doped $(CH)_x$. On the y axis are plotted the parameters t_{mult} and a corresponding average $t_\perp(E_F)$ [specifically, $\frac{1}{2}(t_{\perp,m_1m_2}+t_{\perp,m_1'm_2'})$, where m_1 and m_2 denote nearest neighbors with parallel alignment and m_1' and m_2' denote nearest neighbors with antiparallel alignment], while on the x axis is the dopant density. The dashed line goes through the locus of points at which the band gap between the soliton band and the conduction band closes. To the left and below this line the material has a gap and is thus an insulator, while above and to the right of this line the material has no gap and is thus a metal. The solid line divides the same phases when the chain-dopant interactions are included in the Hamiltonian. These we evaluated using $\varepsilon_d=-4.01$ eV and the chain-dopant coupling parameters for the potassium-doped structure given in Table IV. The solid line is

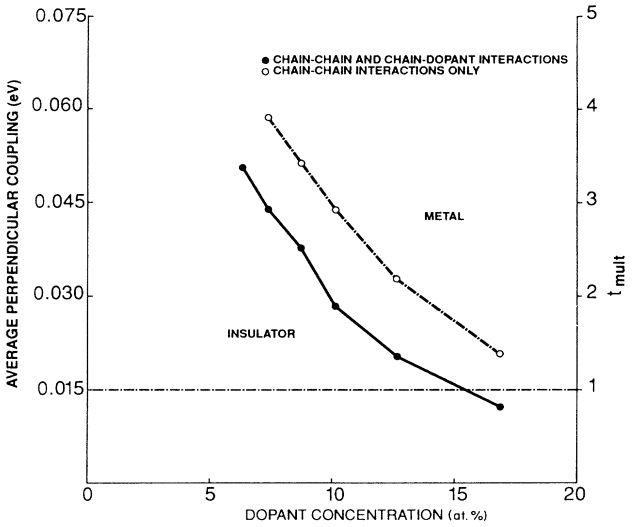

FIG. 5. Phase diagram of the insulator-metal transition calculated for K-doped $(CH)_x$. The solid circles connected by the solid line give the phase boundary when both chain-chain and chain-dopant interactions are included, while the open circles connected by the dashed line give the phase boundary when only chain-chain interactions are included.

TABLE IV. Coupling between dopant ions and chain carbon atoms.

$\lvert n-n'\rvert$	Coupling to sodium atom (eV)	Coupling to potassium atom (eV)
0	1.15	1.78
1	0.77	1.06
2	0.27	0.30
3	0.07	0.06
4	0.01	0.01

below and to the left of the dashed line, which means the transition occurs for smaller dopant densities. This is expected because including the dopant interactions increases the dispersions of the bands. The horizontal dot-dashed line at $t_{\text{mult}}=1$ corresponds to our calculation of interchain coupling in Eqs. (8) and (15). If interchain coupling only gave rise to the insulator-metal transition, then these calculations predict that the transition would occur where the solid line crosses the dot-dashed line, or, more accurately in view of the possible phases of K-doped $(CH)_x$, at 16.7%. This dopant percentage is larger than what is experimentally observed. In order to obtain an insulator-metal transition in K-doped $(CH)_x$ at the observed value of approximately 8%, the interchain coupling must be three times larger than what we have estimated. For sodium-doped polyacetylene even at $y=16.7\%$, $t_{\text{mult}}=7.4$ is required to cause the metallic transition when both chain-chain and chain-dopant coupling is included. We conclude that interchain coupling alone is not the mechanism for the transition in this system.

V. DENSITY OF STATES FOR FINITE CHAINS

The three-dimensional density of states (DOS) has been calculated in the simplest approximation, with only the atoms opposite each other, i.e., $n=n'$, giving the interchain coupling.[3,4] It is clear from the foregoing, however, that other couplings play an important role, complicating the problem of calculating the DOS. Taking advantage of the highly anisotropic nature of $(CH)_x$, we have formulated an approximate method for calculating the energy levels that includes interactions between all the atoms on the chains. This allows us to write analytic forms for the three-dimensional density of states in terms of interchain coupling parameters. The effect of chain-dopant coupling is then taken into account by second-order perturbation theory. We make calculations both with and without the Coulomb potential H_{Coul} in order to study how this term affects the DOS.

Our calculations were done for chains of 108 sites for Na-doped $(CH)_x$ and 104 sites for K-doped $(CH)_x$, which is of the order of the largest coherence length reported. For Na-doped $(CH)_x$, there are three chains in a unit cell, which means if we wish to calculate the band structure exactly, we must solve a 324×324 matrix for each value of $\mathbf{k}_\perp$. With our approximation, we need to solve a 108×108 matrix just once, and then solve 108 3×3 matrices for each value of $\mathbf{k}_\perp$, a much quicker process. Structurally, both undoped and K-doped $(CH)_x$ have two chains per unit cell. However, as we will see, inclusion of only π orbital coupling makes the two nonequivalent chains equivalent, giving one chain per unit cell. Under these circumstances, an analytic expression can be written for the perpendicular dispersion.

We first consider the effect of the term $H_{c\text{-}c}$. Consider two different eigenvectors of energies E and E' on neighboring chains. The coupling between these eigenvectors is given by

$$t_{\perp,mm'}(E,E')=\sum_{n=1}^{N_c}\sum_{n'=1}^{N_c} c_n(E)c_{n'}(E')t^{c\text{-}c}_{nm,n'm'}\ , \qquad (16)$$

where these terms are defined in Sec. II. If the interchain coupling were zero for $n\neq n'$, then $t_{\perp,mm'}$ would be zero unless $E=E'$. However, even when the couplings for $n\neq n'$ dominate, as for polyacetylene, the perpendicular coupling still tends to be orthogonal. This is because the nth chain eigenvectors with different energies have different numbers of nodes, so that contributions from different pairs of sites more or less cancel. The $(CH)_x$ crystal therefore contains N_c states, degenerate with the M_c states on the other chains of the same energy (to zero order in the coupling), but uncoupled to states of different energy. In other words, each of these basis states couples to a like basis state on the other chains to form two-dimensional lattices for the three crystal structures we have been considering (Fig. 6). As noted earlier, those for undoped and K-doped $(CH)_x$ are taken to have only one atom per unit cell. The reason for the reduction is that the Hamiltonian [Eqs. (1)–(5)] contains no information on the orientation of a given chain (that is, anything inside the circles of Fig. 6), but only on how two chains interact. In other words, the two chains in the unit cell are coupled equivalently to their nearest neighbors and are thus indistinguishable for these calculations. For example, the lattices of Figs. 6(a) and 6(c) can be translated by $(a_x/2)\hat{\mathbf{x}}+a_y\hat{\mathbf{y}}$ and $a_x\hat{\mathbf{x}}+a_y\hat{\mathbf{y}}$, respectively, and the original interchain coupling pattern is reproduced. If we included coupling between carbon π orbitals and hydrogen orbitals, that would bring in the backbone electronic states, causing an asymmetry in coupling between opposite bonds and increasing the unit-cell size.

For the coupling between chains we will use the results of Eq. (15), which have been plotted in Fig. 4 for undoped $(CH)_x$. For all three cases shown in Fig. 6 there are only two different coupling strengths between pairs of chains, the stronger coupling indicated by the darker line. The variation of interchain coupling is due to chain separation, chain orientation, and the chain zigzag. For example, in undoped $(CH)_x$, the difference in coupling between the nonequivalent and equivalent chains is due to their different spacing and orientation. The couplings between a chain and the four nonequivalent chains surrounding it are equal because they all have an antiparallel alignment. However, in K-doped $(CH)_x$, chain orientation and separation would give rise to equal couplings; the existence of two different couplings in that case is due to antiparallel

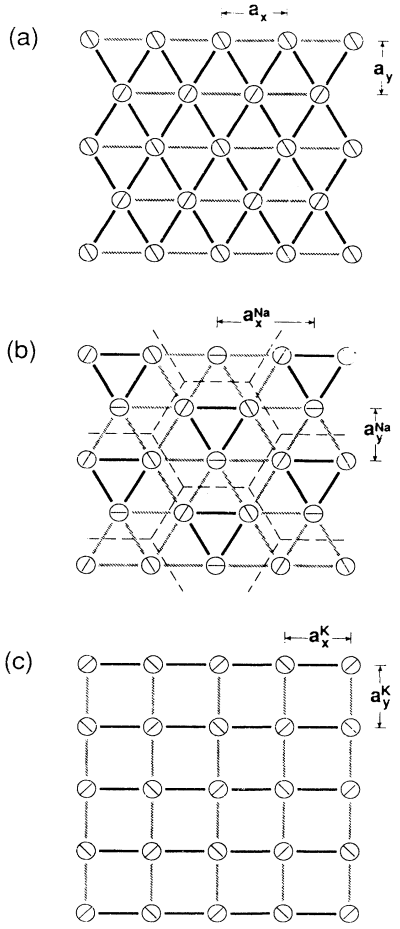

FIG. 6. Two-dimensional lattices of (a) undoped polyacetylene, (b) sodium-doped polyacetylene, and (c) potassium-doped polyacetylene. The circles represent the chains and the lines connecting them represent the interchain coupling, the darkness of the line indicating the strength of the coupling. The dashed line in (b) represents the three-chain unit cell.

alignment for half the chains and parallel alignment for the other half.

For the time being we shall consider the interchain couplings as parameters and calculate the DOS in terms of these parameters. For a two-dimensional lattice in tight-binding theory, the energy for a particular wave vector is found by minimizing that energy with respect to the orbital coefficients. This leads to an eigenvalue equation of the dimension of the number of chains in the unit cell. For one chain per unit cell, we may derive this equation as follows: The three-dimensional wave function with perpendicular wave vector $\mathbf{k}_\perp$ may be written

$$|i,\mathbf{k}_\perp\rangle = M_c^{-1/2} \sum_{m=1}^{M_c} e^{i\mathbf{k}_\perp\cdot\mathbf{r}_m} |i,m\rangle \ , \tag{17}$$

where $|i,m\rangle$ is the one-dimensional eigenvector of energy E_i in unit cell m, $\mathbf{r}_m$ the vector pointing from the origin to unit cell m, and M_c the number of unit cells, in this case equal to the number of chains. The energy of an electron with the wave function (17) may be written

$$E_{i,\mathbf{k}_\perp} = E_i + \sum_{m'} e^{i\mathbf{k}_\perp\cdot(\mathbf{r}_m - \mathbf{r}_{m'})} \langle i,m'|H_{c\text{-}c}|i,m\rangle \ , \tag{18}$$

where the summation is over only the terms for which m' is a nearest neighbor to m.

For undoped polyacetylene, shown in Fig. 6(a), Eqs. (17) and (18) lead to the dispersion perpendicular to the chains:

$$E_{i,\mathbf{k}_\perp} = E_i + 4V_1 \cos\frac{k_x a_x}{2} \cos k_y a_y + 2V_2 \cos k_x a_x \ , \tag{19}$$

where V_1 is the stronger coupling between inequivalent chains and V_2 is the weaker coupling between equivalent chains. Because $V_1 < 0$, the valence-band minimum occurs at $k_x = k_y = 0$ and the maximum (for the direction perpendicular to the chains) at $k_x = 0$, $k_y = \pi/a_y$. This result appears to be in disagreement with the result of the local-density-functional calculations of Vogl and Campbell,[5] where the valence-band maximum was found at $k_x = k_y = 0$. It must be remembered, however, that our Brillouin zone is twice as large as theirs in the y direction because we have taken the unit cell to contain one chain instead of two, as discussed earlier. The halving of the Brillouin zone causes E_k versus k to be bent back (from the zone point D), resulting in the valence-band maximum at $k_y = 0$ (at the point B). The results of our calculation are therefore equivalent to those of Vogl and Campbell. The dispersion or bandwidth in the perpendicular direction obtained from Eq. (19) is $8V_1$. Equation (15) (see also Fig. 4) gives $|V_1| = 0.0204$ eV at the valence-band maximum, leading to the perpendicular bandwidth of 0.16 eV given in Table III. The perpendicular bandwidth obtained in Ref. 5 is about three times as large, presumably due to the enhanced coupling resulting from the inclusion of the hydrogens. The perpendicular bandwidth also gives the lowering of the thermal energy gap E_g due to interchain coupling. However, the direct optical gap is not changed by interchain π band coupling, in contradiction to a previous claim.[37] For k_z at the Brillouin-zone edge, interchain coupling moves the valence-band maximum and the conduction-band minimum in the same direction. The apparent change in the optical gap due to interchain coupling found in Ref. 37, for example, results from the assumption of two chains per unit cell, pointed out earlier to be inconsistent with the use of the Hamiltonian (1)–(5), or the simplified version thereof used in Ref. 37. With this assumption a band splitting is obtained, with two bands moving towards each other. However, the wave functions of the two states moving towards each other are orthogonal and no optical transition can occur between them. Physically, coupling to the H atoms does result in a splitting.[5] Experimental observation of the change of the optical transition energy with pressure, however, cannot give information about π-band–π-band coupling, but only about coupling of the π band to other polyacetylene bands.

For potassium-doped polyacetylene, the perpendicular dispersion found from Eqs. (17) and (18), by considering the lattice in Fig. 6(c), is

$$E_{i,\mathbf{k}_\perp}=E_i+2V_1^{\mathrm{K}}\cos k_x a_x^{\mathrm{K}}+2V_2^{\mathrm{K}}\cos k_y a_y^{\mathrm{K}} , \tag{20}$$

where a_x^{K} and a_y^{K} are defined in the figure and V_1^{K} and V_2^{K} are the couplings appropriate for the potassium-doped structure.

To treat a case with more than one chain per unit cell, we define a Bloch wave function for the jth chain in each unit cell with wave vector $\mathbf{k}_\perp$ and energy E_i:

$$|i,\mathbf{k}_\perp,j\rangle=M_c^{-1/2}\sum_{m=1}^{M_c} e^{i\mathbf{k}_\perp\cdot\mathbf{r}_m}|i,m,j\rangle . \tag{21}$$

The wave function $|i,\mathbf{k}_\perp\rangle$ belonging to the total energy $E_{i,\mathbf{k}_\perp}$ is a superposition of wave functions (21) for each j with constant coefficients $c_{ij,\mathbf{k}_\perp}$:

$$|i,\mathbf{k}_\perp\rangle=\sum_{j=1}^{j_t} c_{ij,\mathbf{k}_\perp}|i,\mathbf{k}_\perp,j\rangle , \tag{22}$$

where j_t is the number of chains in the unit cell. The $c_{ij,\mathbf{k}_\perp}$ are determined by the condition that the energy $E_{i,\mathbf{k}_\perp}$ be a minimum. This leads, as usual, to a set of j_t linear homogeneous equations in the $c_{ij,\mathbf{k}_\perp}$:

$$\sum_{m'=1}^{N}\sum_{j'=1}^{j_t} e^{i\mathbf{k}_\perp\cdot(\mathbf{r}_m-\mathbf{r}_{m'})} \times\langle i,m',j'|H_{\mathrm{SSH}}+H_{c\text{-}c}|i,m,j\rangle c_{ij'k} -E_{i,\mathbf{k}_\perp}c_{ijk}=0 \quad \text{for } j=1,2,\ldots,j_t . \tag{23}$$

The requirement that the set of equations (23) have a nontrivial solution leads to the condition of the vanishing of the j_t by j_t determinant with elements

$$\sum_{m'=1}^{N}\sum_{j'=1}^{j_t} e^{i\mathbf{k}_\perp\cdot(\mathbf{r}_m-\mathbf{r}_{m'})} \times\langle i,m',j'|H_{\mathrm{SSH}}+H_{c\text{-}c}|i,m,j\rangle -E_{i,\mathbf{k}_\perp}\delta_{jj'} , \tag{24}$$

j varying from 1 to j_t. For the case of Na-doped $(CH)_x$, with $j_t=3$ and hexagonal unit cells chosen as shown in Fig. 6(b), the equation for $E_{i,\mathbf{k}_\perp}$ is

$$\begin{vmatrix} -\Delta E_{i,\mathbf{k}_\perp} & g_1 & g_2 \\ g_1^* & -\Delta E_{i,\mathbf{k}_\perp} & g_3 \\ g_2^* & g_3^* & -\Delta E_{i,\mathbf{k}_\perp} \end{vmatrix}=0 , \tag{25}$$

where $\Delta E_{i,\mathbf{k}_\perp}=E_{i,\mathbf{k}_\perp}-E_i$, the change in energy due to interchain coupling, and

$$\begin{aligned} g_1&=V_1^{\mathrm{Na}}+V_2^{\mathrm{Na}}(e^{i(k_x a_x^{\mathrm{Na}}-k_y a_y^{\mathrm{Na}})}+e^{-2ik_y a_y^{\mathrm{Na}}}) ,\\ g_2&=V_1^{\mathrm{Na}}+V_2^{\mathrm{Na}}(e^{-2ik_y a_y^{\mathrm{Na}}}+e^{-i(k_x a_x^{\mathrm{Na}}+k_y a_y^{\mathrm{Na}})}) ,\\ g_3&=V_1^{\mathrm{Na}}+V_2^{\mathrm{Na}}(e^{-i(k_x a_x^{\mathrm{Na}}+k_y a_y^{\mathrm{Na}})}+e^{i(k_x a_x^{\mathrm{Na}}-k_y a_y^{\mathrm{Na}})}) . \end{aligned} \tag{26}$$

Solutions of Eq. (25) with Eq. (26) give three values of $\Delta E_{i,\mathbf{k}_\perp}$, thus of $E_{i,\mathbf{k}_\perp}$, to be distinguished by superscripts (a), (b), and (c). These values, substituted into Eq. (23) for the $c_{ij,\mathbf{k}_\perp}$, lead to three sets of $c_{ij,\mathbf{k}_\perp}$'s to be denoted $c_{ij,\mathbf{k}_\perp}^{(a)}$, $c_{ij,\mathbf{k}_\perp}^{(b)}$, and $c_{ij,\mathbf{k}_\perp}^{(c)}$.

We now turn to the additional shift in chain energy caused by coupling to the dopants, represented by the Hamiltonian Eq. (9). Because there is no first-order matrix element of Eq. (9) for a state representing a given chain, the energy correction due to the dopants must be obtained with second-order perturbation theory. For specificity, we consider the sodium-doped geometry, where there are three chains and one ion column in the unit cell. Taking as zero-order wave functions $|i,\mathbf{k}_\perp\rangle$ of Eq. (22), with a set of $c_{ij,\mathbf{k}_\perp}$'s determined by solving Eq. (23) with an $E_{i,\mathbf{k}_\perp}$ obtained from Eq. (25), we have a nondegenerate set. Second-order perturbation theory then gives the energy correction for $E_{i,\mathbf{k}_\perp}^{(a)}$:

$$W_{i,(a)}^{(2)}=\frac{\sum_{n'=1}^{N_d}|H'_{i,(a);n'}|^2}{E_{i,\mathbf{k}_\perp}^{(a)}-\varepsilon_d} , \tag{27}$$

where ε_d is the energy level on the ion and the summation is taken over the ions in a column. Similar expressions hold, of course, for the (b) and (c) linear combinations.

Because the three chains in the unit cell are located symmetrically with respect to the ion column, the matrix element may be written

$$H'_{i,(a);n'}=D_{in'}(c_{i1,\mathbf{k}_\perp}^{(a)}+c_{i2,\mathbf{k}_\perp}^{(a)}+c_{i3,\mathbf{k}_\perp}^{(a)}) , \tag{28}$$

where

$$D_{in'}=\sum_{n=1}^{N_c} t_{n,m;n',m'}^{c\text{-}d}c_n(E_i) , \tag{29}$$

giving the coupling of ion n' to chain eigenvector i. For K-doped $(CH)_x$, the presence of the dopant breaks the symmetry and there are now two chains per unit cell. One chain has a dopant column to the side, and the other chain has a dopant column above. An analogous expression to Eq. (28) for two chains must be used.

To obtain a measure of the ion-chain coupling, we introduce the quantity $t_{\perp,mm'}^{c\text{-}d}(E)$, the effective perpendicular coupling between a chain m and an ion column m'. In the spirit of second-order perturbation theory, we take

$$t_{\perp,mm'}^{c\text{-}d}(E)=\frac{1}{E-\varepsilon_d}\sum_{n'=1}^{N_d}\left[\sum_{n=1}^{N_c} c_n(E)t_{n,m;n'm'}^{c\text{-}d}\right]^2 . \tag{30}$$

To evaluate $t_{\perp,mm'}^{c\text{-}d}(E)$ the quantity $t_{n,m;n',m'}^{c\text{-}d}$ was calculated as described in Sec. II. The results are plotted as a function of energy, in the absence of a Coulomb potential, for 8.33% sodium doping in Fig. 7. The coupling to the ion column is large at low energies where the coupling to different ions tends to reinforce. In addition, even though the ions are much closer than the neighboring chains, their perturbation is of the same order of magnitude. This occurs because the energy difference be-

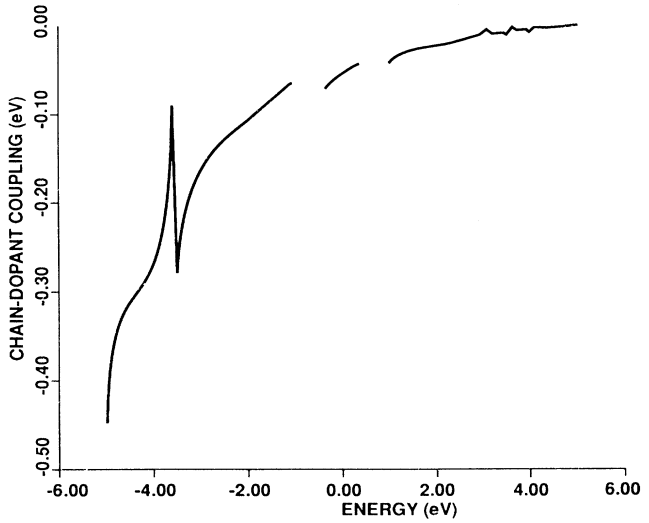

FIG. 7. $t^{c\text{-}d}_{\perp,mm'}$ as a function of energy calculated from Eq. (30) for 8.33% Na doping. The Coulomb potential is neglected.

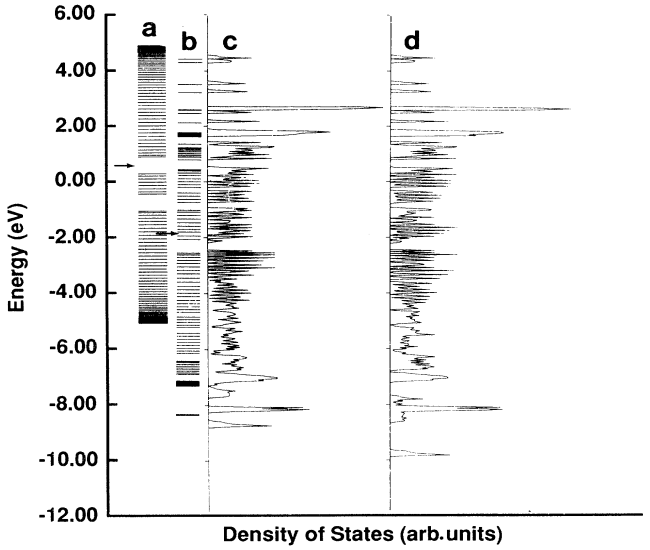

FIG. 8. Energy levels and density of states for a 104-site chain of 8.33% Na-doped $(CH)_x$ calculated from (a) H_{SSH}, (b) $H_{SSH}+H_{Coul}$, (c) $H_{SSH}+H_{Coul}+H_{c\text{-}c}$, (d) $H_{SSH}+H_{Coul}+H_{c\text{-}c}+H_{c\text{-}d}$. The arrows indicate E_F measured with respect to the C p_z orbital energy.

tween the carbon p orbitals and the ion s orbitals, which decrease the coupling, balances out the increased hopping parameter due to the proximity of the ion. The discontinuity at $E=-3.6$ eV occurs because at that energy the nodes of the chain wave function are aligned with the ion positions. Addition of the Coulomb potential gives $t^{c\text{-}d}_{\perp,mm'}(E)$ more structure as a function of energy, but does not significantly change its magnitude.

To show explicitly the effect on the chain energy E_i (calculated with H_{SSH}) of chain-chain and chain-dopant coupling, we write the energy for the state $i(a)$ including these effects by incorporating Eqs. (28) and (27):

$$E_i^{(a)}=E_i+\Delta E^{(a)}_{i,\mathbf{k}_\perp}+\frac{\sum_{n'=1}^{N_d} D^2_{in'}|c_{i1,\mathbf{k}_\perp}+c_{i2,\mathbf{k}_\perp}+c_{i3,\mathbf{k}_\perp}|^2}{E_i+\Delta E^{(a)}_{i,\mathbf{k}_\perp}-\varepsilon_d}\ . \tag{31}$$

Similar relations may be written for the states (b) and (c) of the Na-doped lattice.

To evaluate (31) numerically, $D_{in'}$ was calculated from Eq. (29). $\Delta E^{(a)}_{i,k_\perp}$ and $c^{(a)}_{ij,\mathbf{k}_\perp}$ were calculated from Eqs. (25) and (23), respectively. V_1 and V_2 were taken from Eq. (15). The dopant orbital energies are $\varepsilon_d=-4.95$ eV for Na and -4.01 eV for K.

The DOS versus energy, including both the effects of chain-chain and chain-dopant coupling, was calculated by evaluating Eq. (31) for a large number of perpendicular wave vectors sampled uniformly across the Brillouin zone, and plotting a histogram of the energies, with the bin size chosen small enough to make the plots appear continuous. To show separately the effects of chain-chain coupling on the DOS versus energy, we followed the same procedure using Eq. (20) or (25), as required, instead of Eq. (31). The resulting DOS for Na-doped $(CH)_x$ is plotted in Figs. 8 and 9, while that for K-doped $(CH)_x$ is plotted in Figs. 10 and 11. The lowering of all the energy levels going from Figs. 8(a) to 8(b) or Figs. 10(a) to 10(b) is due to the potential well, as has been discussed in Refs. 27 and 28. Figures 8(c) and 10(c) show the spreading of the discrete levels due to interchain coupling only. As anticipated, the spreading is larger for the lower energy levels, making the valence bands quite continuous for K-doping and relatively so for Na doping. The difference is due to the different geometries. For the Na doping case, although there is a perpendicular coupling of approxi-

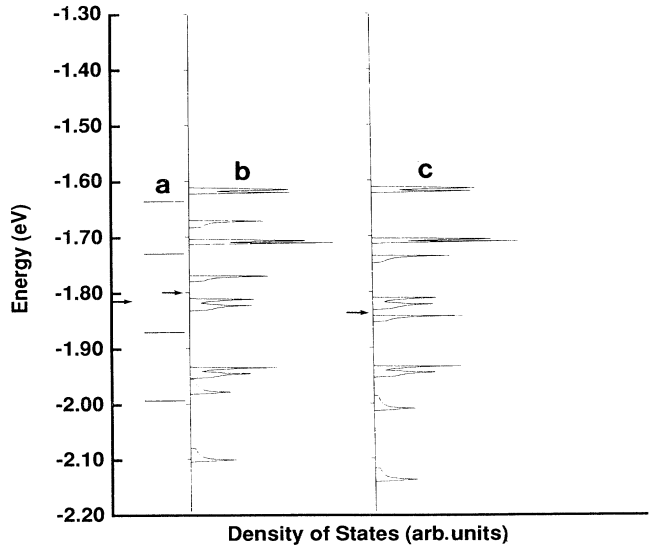

FIG. 9. Higher-resolution histogram of the DOS in Fig. 8 in the neighborhood of E_F. The DOS is calculated from (a) $H_{SSH}+H_{Coul}$, (b) $H_{SSH}+H_{Coul}+H_{c\text{-}c}$, (c) $H_{SSH}+H_{Coul}+H_{c\text{-}c}+H_{c\text{-}d}$.

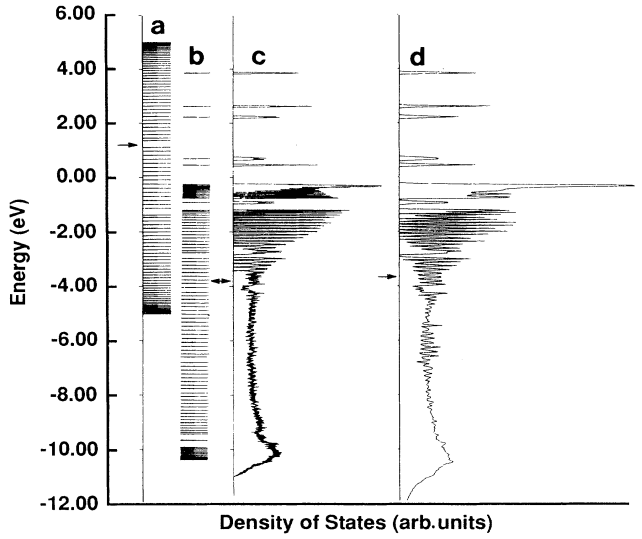

FIG. 10. Energy levels and density of states for a 108-site chain of 16.7% K-doped $(CH)_x$ calculated from (a) H_{SSH}, (b) $H_{SSH}+H_{Coul}$, (c) $H_{SSH}+H_{Coul}+H_{c\text{-}c}$, (d) $H_{SSH}+H_{Coul}+H_{c\text{-}c}+H_{c\text{-}d}$. The arrows indicate E_F measured with respect to the C p_z orbital energy.

mately 100 meV between any pair of the three chains surrounding an ion column, the coupling between these three and other chains is an order of magnitude less. Therefore, there is not a significant dependence on the perpendicular wave vector and the peaks are not significantly broadened. As seen from a comparison of Figs. 9(b) and 9(c), incorporating dopant-chain coupling gives a shift in the levels, but no increase in dispersion.

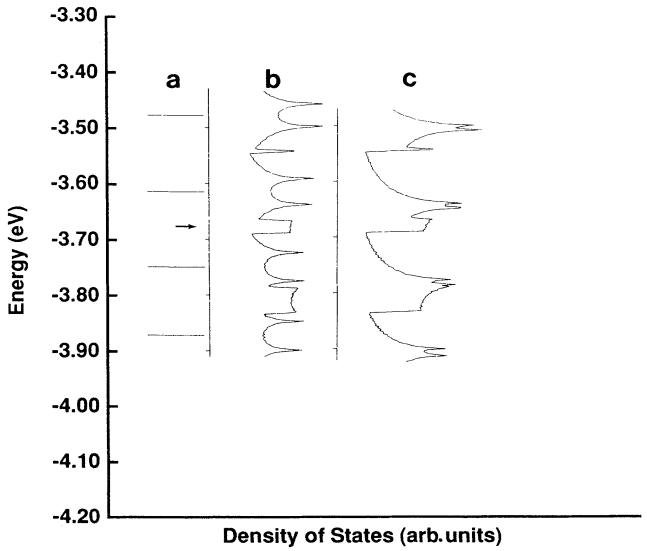

FIG. 11. Higher-resolution histogram of the DOS of Fig. 10 in the neighborhood of E_F. The DOS is calculated from (a) $H_{SSH}+H_{Coul}$, (b) $H_{SSH}+H_{Coul}+H_{c\text{-}c}$, (c) $H_{SSH}+H_{Coul}+H_{c\text{-}c}+H_{c\text{-}d}$.

Figures 9 and 11 show clearly that there remains a small gap at the Fermi energy for the Na-doping case even when both chain-chain and chain-dopant interactions are included, but the energy levels are continuous at E_F for the K doping. The difference may again be entirely due to the difference in geometry, but it must be remembered that the K-doping concentration is twice as high as the Na-doping concentration. The smaller doping results in the potential well for the Na-doping material being shallower by almost a factor of 2, and also decreases the soliton wave-function overlap. The pairs of singularities seen in the DOS of Fig. 11(b) for K doping, symmetric about the original discrete levels shown in Fig. 11(a), are expected to arise from a two-dimensional lattice with anisotropic coupling in the two perpendicular directions. The flat-topped peaks between the singularities arise from the overlap in the DOS from two different discrete states. Again, as seen in Fig. 11(c), the dopant-chain coupling shifts all the energies downward, but does not increase the perpendicular bandwidth.

VI. CONCLUSIONS

We have developed here a model to examine three-dimensional effects in undoped and doped $(CH)_x$. Our results for the band structure of undoped $(CH)_x$ lie in the range delineated by past calculations, allowing confidence in our calculations for the doped material. The calculations use the experimentally determined geometry of the crystal and can be extended to other structures we did not consider here as well as other polymers. We find that opposite neighbors may account for as little as 30% of the interchain coupling in $(CH)_x$. Inclusion of next nearest neighbors brings it up to 75% of the coupling. An important result obtained in the paper is that the magnitude of the interchain coupling is quite energy dependent, decreasing monotonically from a maximum value at the bottom of the valence band. Thus, for example, for the more strongly coupled chains, the equivalent ones $|t_\perp| \simeq 0.03$ eV at the Fermi energy, considerably weaker than the 0.1-eV value usually assumed. This was shown for undoped material in Fig. 4 and is also true for doped material. Although $t_\perp$ changes when $(CH)_x$ is doped due to the change in lattice structure, the change is small, particularly at E_F. Coupling between a $(CH)_x$ chain and a potassium or sodium ion column also has maximum magnitude at the bottom of the valence band, being several times as large as the chain-chain coupling at that energy. That coupling also decreases (although not monotonically) with energy to a small value, comparable to that for interchain coupling at E_F and above.

Incorporating the couplings we have calculated to find the energy-level structure, we find characteristic differences between Na-doped and K-doped $(CH)_x$. Because of its structure, for the Na-doped $(CH)_x$ there is small coupling between the three chains surrounding a Na ion column and other chains, resulting in little broadening of the levels by interchain interaction and a transverse bandwidth at E_F [see Figs. 9(b) or 9(c)] less than 0.1 eV. K-doped $(CH)_x$ has a somewhat larger

transverse bandwidth, 0.15 eV according to Figs. 11(b) or 11(c). This bandwidth is slightly smaller than the one we found for undoped $(CH)_x$. The larger anisotropy of metallic material than undoped material was also found in optical properties, specifically for AsF_5 doping.[38] The small transverse bandwidth in the metallic state suggests that transverse conductivity in that state is due to diffusive hopping rather than band motion, at least for Na doping and K doping.

In principle, interchain coupling itself could shrink the energy gap between soliton band and conduction band to zero. We found that to account for the insulator-metal transition occurring at $\sim 6\%$ would require much stronger interchain coupling than is characteristic of $(CH)_x$. The interchain and chain-dopant coupling we calculate will not stabilize a polaron lattice in the metallic state against a Peierls distortion, in contradiction to the suggestion of Lögdlund *et al.*[39] We reach this conclusion because $t_\perp^{c\text{-}c}(E_F)$ and $t_\perp^{c\text{-}d}(E_F)$ are essentially equal to $t_\perp^{c\text{-}c}(E_F)$ in an undoped sample, and it is evident that chain-chain coupling does not prevent the Peierls distortion in an undoped sample of $(CH)_x$.

[1]W. P. Su, J. R. Schrieffer, and A. J. Heeger, Phys. Rev. B **22**, 2099 (1980).

[2]D. Baeriswyl and K. Maki, Synth. Met. **28**, D507 (1989).

[3]D. Baeriswyl and K. Maki, Phys. Rev. B **28**, 2068 (1983).

[4]D. Baerswyl and K. Maki, Phys. Rev. B **38**, 8135 (1988).

[5]P. Vogl and D. K. Campbell, Phys. Rev. Lett. **62**, 2012 (1989), and references therein.

[6]A. J. Heeger, S. Kivelson, J. R. Schrieffer, and W.-P. Su, Rev. Mod. Phys. **60**, 781 (1988), p. 840.

[7]P. M. Grant and I. P. Batra, J. Phys. (Paris) Colloq. **44**, C3-437 (1983).

[8]J. Ashkenazi, E. Ehrenfreund, Z. Vardeny, and O. Brafman, Mol. Cryst. Liq. Cryst. **117**, 193 (1985).

[9]R. H. Baughman, S. L. Hsu, L. R. Anderson, G. P. Pez, and A. J. Signorelli, *Molecular Metals,* Vol. 1 of *NATO Conference Series, Series VI,* edited by W. E. Hatfield (Plenum, New York, 1979), p. 187.

[10]S. Stafström, Phys. Rev. B **32**, 4060 (1985).

[11]P. L. Danielson and R. C. Ball, J. Phys. (Paris) **46**, 131 (1985).

[12]K. Fesser, Phys. Rev. B **40**, 1962 (1989).

[13]P. L. Danielson, J. Phys. C **19**, L741 (1986).

[14]S. A. Brazovskii, L. D. Gor'kov, and J. R. Schrieffer, Phys. Scr. **25**, 423 (1982).

[15]M. Kertesz, Int. J. Quantum Chem. **29**, 1165 (1986).

[16]J. L. Brédas, B. Thémans, J. G. Fripiat, J. M. André, and R. R. Chance, Phys. Rev. B **29**, 6761 (1984).

[17]H. Takayama, Y. R. Lin-Liu, and K. Maki, Phys. Rev. B **21**, 2388 (1980).

[18]F. Morales, J. Chen. T.-C. Chung, and A. J. Heeger, Synth. Met. **11**, 271 (1985).

[19]R. H. Baughman, N. S. Murthy, G. G. Miller, L. W. Shacklette, and R. M. Metzger, J. Phys. (Paris) Colloq. **44**, C3-53 (1983).

[20]R. H. Baughman, L. W. Shacklette, N. S. Murthy, G. G. Miller, and R. L. Elsenbaumer, Mol. Cryst. Liq. Cryst. **118**, 253 (1985).

[21]J. P. Pouget, in *Electronic Properties of Polymers and Related Compounds,* edited by H. Kuzmány, M. Mehring, and S. Roth (Springer-Verlag, New York, 1985), p. 26.

[22]D. Tanner, G. Doll, K. Rao, C. Eklund, G. Arbuckle, and A. G. MacDiarmid, Synth. Met. **28**, D141 (1989).

[23]H.-Y. Choi and E. J. Mele, Phys. Rev. B **34**, 8750 (1986).

[24]A. E. Jacobs, W. G. Macready, K. Y. Szeto, and K. Makì, Phys. Rev. B **41**, 3647 (1990).

[25]E. Conwell, Phys. Rev. B **33**, 2465 (1986).

[26]S. Stafström and J.-L. Brédas, Phys. Rev. B **38**, 4180 (1988).

[27]E. M. Conwell, H. A. Mizes, and S. Jeyadev, Phys. Rev. B **40**, 1630 (1989).

[28]E. M. Conwell, H. A. Mizes, and S. Jeyadev, Phys. Rev. B **41**, 5067 (1990).

[29]E. M. Conwell, H. A. Mizes, and S. Jeyadev, in *Advanced Organic Solid State Materials,* edited by Long Y. Chiang, Paul M. Chaikin, and Dwaine O. Cowan, MRS Symposia Proceedings No. 173 (Materials Research Society, Pittsburgh, 1990), p. 409.

[30]H. Kahlert, O. Leitner, and G. Leising, Synth. Met. **17**, 467 (1987).

[31]M. Winokur, Y. B. Moon, A. J. Heeger, J. Barker, D. C. Bott, and H. Shirakawa, Phys. Rev. Lett. **58**, 2329 (1987).

[32]J. Kouteck and J. Paldus, Tetrahedron **19**, Suppl. 2, 201 (1963).

[33]W. Harrison, *Electronic Structure and the Properties of Solids* (Freeman, San Francisco, 1980).

[34]W. A. Harrison, Phys. Rev. B **24**, 5835 (1981).

[35]M. J. Rice and E. J. Mele, Chem. Scr. **17**, 121 (1981).

[36]N. Nakahara and K. Maki, Phys. Rev. B **24**, 1045 (1981).

[37]See, for example, D. Moses, A. Feldblum, E. Ehrenfreund, A. J. Heeger, T.-C. Chung, and A. G. MacDiarmid, Phys. Rev. B **25**, 3361 (1982).

[38]G. Leising, Phys. Rev. B **38**, 10 313 (1988).

[39]M. Lögdlund, R. Lazzaroni, S. Stafström, W. R. Salaneck, and J.-L. Brédas, Phys. Rev. Lett. **63**, 1841 (1989).